

Study on Preparation and Electrochemical Properties of Biomass-Derived Spherical Activated Carbon

Yuzhu Ma^{1,2,*}, Cong Zhou³, Baojun Yu^{1,2}, Mingming Chen^{1,2}, Chengyang Wang^{1,2}

¹Key Laboratory for Green Chemical Technology of Ministry of Education, School of Chemical Engineering and Technology, Tianjin University, Tianjin, P. R. China

²Collaborative Innovation Center of Chemical Science and Engineering (Tianjin), Tianjin, P. R. China

³Key Laboratory for Energy Conversion and Storage Materials, College of Chemistry, Beijing Normal University, Beijing, China

Email address:

mayuzhu01@126.com (Yuzhu Ma)

*Corresponding author

To cite this article:

Yuzhu Ma, Cong Zhou, Baojun Yu, Mingming Chen, Chengyang Wang. Study on Preparation and Electrochemical Properties of Biomass-Derived Spherical Activated Carbon. *American Journal of Modern Energy*. Vol. 4, No. 4, 2018, pp. 26-32.
doi: 10.11648/j.ajme.20180404.11

Received: October 25, 2018; **Accepted:** December 4, 2018; **Published:** January 3, 2019

Abstract: Spherical activated carbon (SPs) with hierarchical porous structure was prepared via a simple solvent evaporation method followed by an activation process using leonardite humic acid (LHA) as carbon source. The surface morphologies and pore parameters of the as-prepared SPs were analyzed by scanning electron microscope (SEM) and N₂ physical adsorption-desorption instrument. The electrochemical performance of supercapacitors tested by galvanostatic charge-discharge (GCD), cyclic voltammograms (CV) and electrochemical impedance spectroscopy (EIS) are conducted in both aqueous and organic electrolyte. The SPs with high specific surface area (2034 m² g⁻¹) and pore volume (1.24 cm³ g⁻¹) exhibit a superior higher specific capacitance of 319 F g⁻¹ at a current density of 0.05 A g⁻¹ in aqueous electrolyte compared with powdered activated carbon (SP1). In addition, SPs1 also exhibit a high initial specific capacitance of 154 F g⁻¹ at 0.05 A g⁻¹ and a higher capacitance retention of 96.4% than the bulked sample started from the same raw materials in organic electrolyte. These results suggest that the LHA-based spherical activated carbon should be a competitive and promising supercapacitor electrode material.

Keywords: Humic Acid, Spherical Activated Carbon, Pore Structure, Supercapacitors

1. Introduction

Resource depletion and environmental pollution have led to the worldwide activity to develop more sustainable and cleaner energy resources [1, 2]. In this regard, supercapacitors with excellent power density, long cycle life and superior reversibility [3] are one of the electrochemical energy storage devices, which store electricity in electrochemical processes [4]. However, the relatively low energy density and narrow working voltage range also restrain the further development of supercapacitors. Numerous efforts have been devoted to develop novel and high-performance electrode materials with the aim to realize high-efficiency energy storage [4].

Activated carbon is one of the most widely used electrode materials, while the slow ion transportation in the small micropores limits their effective utilization [5]. The spherical

activated carbon with systematically tailored pore structure is an important class of porous materials [6, 7]. It shows various advantages, such as good sphericity, mechanical stability, high thermal conductivity, and good electrical conductivity, et al. These features make them widely used in catalysis, environmental applications, absorbents, especially in energy storage [8-11]. Most importantly, spherical activated carbon with hierarchical porous structure can facilitate ion transport and shorter diffusion pathways, which could display better performance as supercapacitor electrodes and significantly increase the specific capacitance [12]. Therefore, because of their good charge-discharge characteristics, long cycle life, spherical activated carbon has received extensive attention from academia and industry.

As a green renewable and cheap amphiphilic biomass material, Leonardite humic acids (LHA) were employed as

carbon precursor [13]. The unique natural composite materials are typically viewed as a complex mixture of alkyl skeletons and organic chainlike molecule species. LHA as an amphiphilic biomass precursor could be well dispersed in a base solution. Meanwhile, the aromatic ring structure can control the skeleton structure of activated carbon during the activation process, and heteroatoms (including S, N and O) of LHA can also provide more active sites to facilitate the formation of hierarchical porous architecture [14].

Herein, hierarchical spherical porous carbon (SPs) were prepared using LHA as precursor by the efficient and facile solvent evaporation method under ambient pressure. Our strategy offers at least three advantages: (1) the dimethicone has some surface activity, SPs with good dispersity can be obtained without adding any surfactant; (2) the pore structure was high developed through activation process using a small amount of KOH; and (3) hierarchical porous framework provides the pathway to ensure easy accessibility of electrolyte. Furthermore, the electrochemical performances of the optimized SPs were also characterized.

2. Experimental

2.1. Preparation of SPs

The biomass-based LHA acts as main raw material. Pure

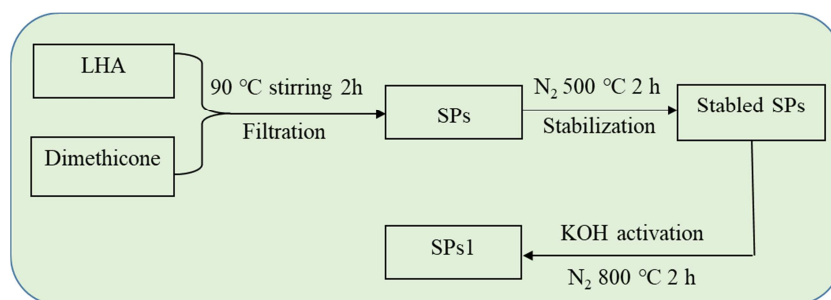


Figure 1. The preparation of spherical activated carbon.

2.2. Supercapacitor Assembly

The double-layer capacitor is composed of electrode, electrolyte, diaphragm, collector fluid and encapsulating element. To fabricate the electrodes, a certain amount of activated carbon material (active material), polytetrafluoroethylene (PTFE) and acetylene black were weighed according to the mass ratio of 8:1:1. Then add ethanol to cover the material and ultrasonic dispersion for 0.5 h. After dried at 50°C for 2 h the electrode materials were repeatedly pressed to form a film with a thickness of 40~60 mm and punched into a circular pole piece with a diameter of 13 mm. The coin type cells of symmetrical supercapacitors (R2430) were assembled using 6 M KOH aqueous solution and 1 M TEABF₄/PC as electrolytes, respectively.

2.3. Characterization

The morphology and microstructure of obtained samples were characterized by FEI NanoSEM 430 scanning electron microscopy (SEM). Nitrogen sorption isotherms were measured

LHA were processed by alkali-solution and acid-isolation method reported previously [21]. Then 10 ml 10% LHA solution (10 g LHA+90 g H₂O+1 ml Ethylenediamine (Ethylenediamine destroys intramolecular hydrogen bonds)) was added into 500 ml dimethicone. After magnetic stirring for 2 h at 90°C (to sufficiently evaporate the water) the black solid was collected at room temperature and washed five times with hexane. The precipitate was dried at 60°C in oven to obtain the spherical carbon (SPs). Then, the resultant SPs were precarbonized at 500°C for 2 h with a heating rate of 2°C min⁻¹ under N₂ atmosphere. Finally, the stabilized SPs was mixed with the KOH solution (alkali/carbon=1:1, mass ratio) and carbonized again using the following heating program: ramped at 2°C min⁻¹ to 800°C and held for 1 h, then cooled naturally to room temperature, washed with diluted HCl, followed by distilled water, and dried at 80°C for 12 h. The final product was labeled SPs1. The specific process is shown in Figure 1. For comparison, pure LHA were directly mixed with the KOH solution (KOH/LHA mass ratio = 1:1). After drying in air, the mixtures were treated with the same procedure above; the obtained activated carbon was named as SP1. In this way, the differences in electrochemical application between spherical activated carbon and powder activated carbon were analyzed.

at 77 K with a Micromeritics Tristar 3000 analyzer. The Brunauer-Emmett-Teller (BET) method was utilized to calculate the specific surface areas (S_{BET}) using adsorption data, the total pore volume was calculated according to the adsorption amount at the relative pressure (P/P_0) of 0.99, and the pore size distribution was calculated through the density function theory (DFT). Galvanostatic charge-discharge (DCG) experiments were performed on an Arbin MSTAT and Land instrument. Cyclic voltammetry (CV) experiments and electrochemical impedance spectroscopy (EIS) were recorded in Princeton PARSTAT2273 electrochemical system. The specific capacitance (C : F g⁻¹) of a single electrode was calculated from the discharge part of galvanostatic charge/discharge curves according to formula1:

$$C = 2It/Vm \quad (1)$$

where V presents the potential change in discharge (0 to 1.0 V for aqueous solution and 0 to 2.7 V for the organic solution, respectively); I is the discharge current (A) and t for the discharge time (s); and m is the mass (g) of activated carbon in

a single electrode.

3. Results and Discussion

3.1. Structural Characterization

The morphology and microstructure were investigated by the SEM. Figure 2a shows that the SPs prepared by solvent evaporation possess regular sphericity and are well dispersed with a diameter of 3-10 μm . It is obvious that there are no obvious changes after KOH activation, while, due to the

etching of the strong alkali of KOH, some certain pores appeared on the surface of SPs1 (Figure 2b). That is because K^+ can become potassium vapor at 800°C, which can spread and etch the material surface, thereby to regulate the channels, and since less alkali is used, it does not damage the morphology of the material. By contrast, although the activated area of the SP1 is larger than that of SPs1, the powdered SP1 (Figure 2c) appears to be irregular without any regular physical structure, which generated a plurality of macropores during the activation process.

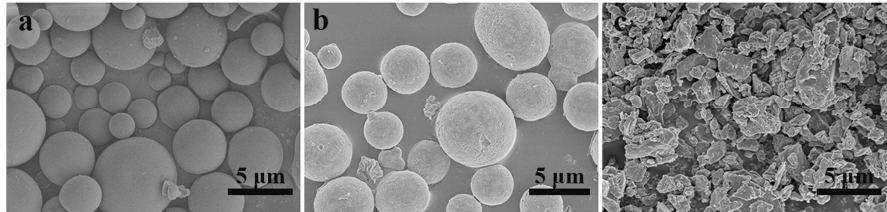


Figure 2. SEM images of samples: (a): SPs; (b): SPs1; (c): SP1.

Figure 3 shows the nitrogen adsorption and desorption isotherms and the pore size distribution curves for the two samples. N_2 adsorption-desorption measurements reveal that SPs1 and SP1 all show type II/IV curve with the hysteresis loop and sharp increase in the N_2 adsorption amount at relatively high pressure (P/P_0 approaches to 1) [15]. Compared with SP1, SPs1 show more N_2 adsorption under relatively low pressure ($P/P_0 < 0.1$), indicating an increase in micropores through activation process. Both of the two samples have relatively obvious hysteresis loop under medium pressure, revealing that the samples have

mesoporous structure. The observed vertical tails at relatively high pressure (P/P_0 near 1.0) is the typical features of macropores, caused by the accumulation of some salt particles [16]. Figure 3b shows that the pore size of SPs1 and SP1 samples is mostly under 10 nm. SPs1 has a relatively uniform pore size of 3.0 nm, larger than that of SP1 (1.5 nm, mostly are micropores). Meanwhile, although the pore size distribution of SP1 is wider than that of SPs1, it is mainly focus on some large and medium holes, which showed limited contribution to capacitance characteristics.

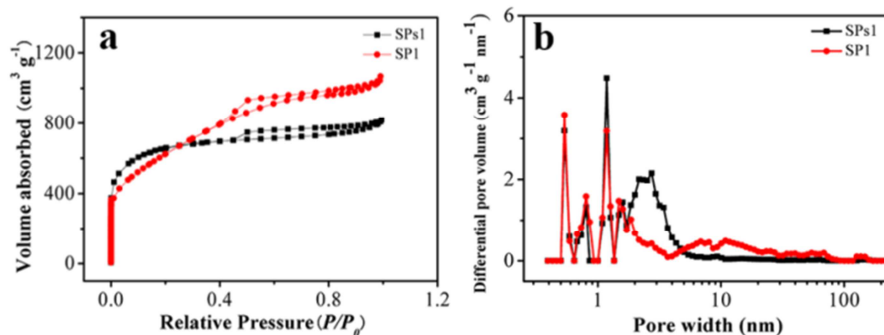


Figure 3. (a) Adsorption/desorption isotherms of N_2 and (b) pore size distribution of different samples.

It can be seen from table 1 that both of the two samples have relatively large specific surface area (2266 $\text{m}^2 \text{g}^{-1}$ for SP1 and 2034 $\text{m}^2 \text{g}^{-1}$ for SPs1, respectively) after being activated by the same amount of KOH. That is because LHA act as an

amphiphilic carbon material can well wetted in a KOH solution, which can lead to homogenized activation. Thus, although activated by the same amount of alkali, the specific surface area of SP1 is larger than that of SPs1.

Table 1. Porosity parameters and Specific surface area of SPs1 and SP1.

Samples	$S_{\text{BET}}^a \text{ m}^2 \text{g}^{-1}$	$V_t^b \text{ cm}^3 \text{g}^{-1}$	$V_{\text{mf}}^c \text{ cm}^3 \text{g}^{-1}$	$V_{\text{me}}^d \text{ cm}^3 \text{g}^{-1}$	$D_{\text{Ae}} \text{ nm}$
SPs1	2034	1.24	0.45	0.64	2.38
SP1	2266	1.93	0.65	0.58	3.32

a BET surface area

b Total pore volume measured at $P/P_0 = 0.99$

c Micropore volume calculated using the t-plot method

d Mesopore volume obtained using the BJH method

e Average pore width determined using the formula $4V_t/S_{\text{BET}}$

3.2. Electrochemical Performance

3.2.1. Electrochemical Performance in Aqueous Electrolyte

Electrochemical performance of the two samples was investigated in 6 M KOH solution. Figure 4a shows the CV curves of the samples at the scan rates of 400 mV s^{-1} in aqueous solution. Obviously, under the high sweep rates of 400 mV s^{-1} , the CV curve of SP1 presents an irregular rectangle shape, while the curve of SPs1 is nearly rectangle shape without redox peaks, indicating the electrical charge and discharge responses are highly reversible [17]. At the same time, the larger area under the CV curve indicates that the SPs1 has stronger electrochemical responses than that of the SP1 powder, which show that SPs1 has good bilayer capacitance characteristics.

Figure 4b shows the galvanostatic charge-discharge (DCG) cycles of the two samples in the potential range of 0 to 1.0 V for aqueous solution. The curves are highly linear and symmetrical indicating nearly perfect capacitive behavior. The high reversibility of the DCG process indicates that the electrode process is mainly focus on the charge transfer in the electric double layer capacitor, and almost no Faraday reaction occurs [18].

The specific capacitances of the SPs1 and SP1 were calculated from the discharge curves and are shown in Figure 4c, respectively. The specific capacitance of SPs1 and SP1

samples is 319 F g^{-1} and 288 F g^{-1} at a current density of 0.05 A g^{-1} , respectively, and the SPs1 electrode can still remain 190 F g^{-1} at the high current density of 100 A g^{-1} , while the SP1 electrode is only 161 F g^{-1} . These results indicate that the utilization rate of micropores in spherical activated carbon is more efficient in energy storage. With the increasing current densities, relatively more micropores could give rise to higher resistance, leading to the decrease of capacitance from micropores. However, the mesopores can provide a transmission channel for electrolyte ions, so the specific capacitances of SP1 (less mesopores) with more micropores decreases faster [19, 20].

To further analyze the electrochemical performance of the SPs1 and SP1, EIS analysis was carried out, as shown in Figure 4d. Compared with SP1, the smaller diameter of semicircle at higher frequencies implies the lower charge transfer resistance of SPs1. In addition, 45° oblique line of SPs1 sample in middle frequency region is not obvious, implying the hierarchical pore structure plays a very important role in the diffusion of electrolyte in the mesopores [21, 22]. The Nyquist plots of all samples had a better vertical line in the low-frequency region, indicating that the activated carbon electrode had an ideal ions and electron transfer efficiency. The ESR values of the two samples are 0.19Ω for SPs1 and 0.24Ω for SP1, respectively.

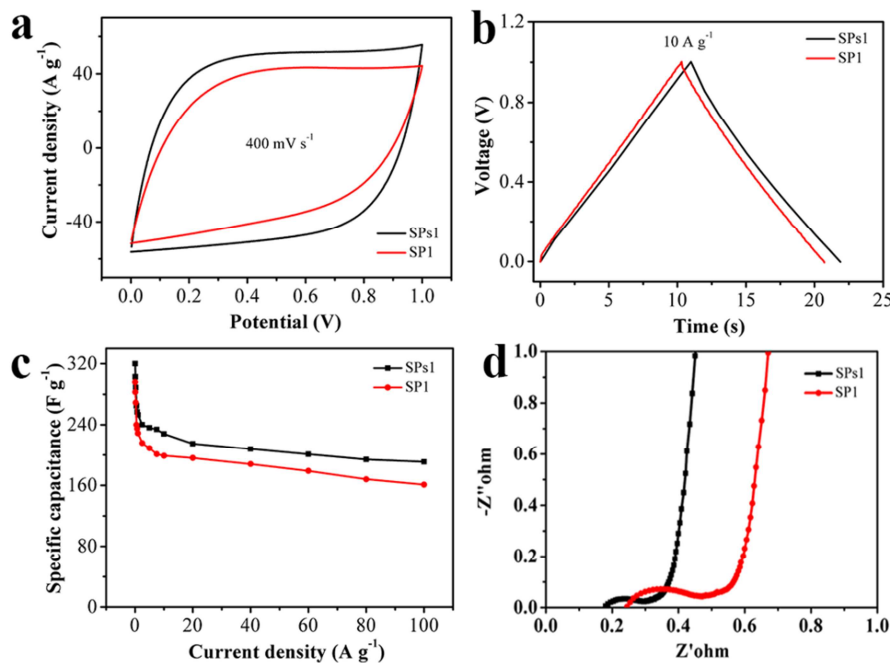


Figure 4. Electrochemical performance of the electrodes in 6 M KOH: (a) CV curves of SPs1 and SP at scan rate of 400 mV s^{-1} ; (b) Charge and Discharge curves at the current density of 10 A g^{-1} ; (c) Rate performance of samples; (d) Nyquist plots for samples.

It's worth noting that after after 10,000 cycles at a current density of 10 A g^{-1} , as shown in Figure 5a, the as-prepared SPs1 electrodes exhibit a capacitance retention ratio of 98.9%, much higher than that of SP1 (capacitance retention: 96.4%). Figure 5b shows the Ragone plots of the SP1 and SPs1 in aqueous electrolytes. In the aqueous electrolyte, the SPs1 electrode had a maximum energy density of 10.28 Wh kg^{-1} ,

much higher than that of SP1 (7.6 Wh kg^{-1}). Furthermore, the SPs1 exhibited the stablest performance with an energy density of 4.08 Wh kg^{-1} at the high-power density of 19.82 kW kg^{-1} in the aqueous electrolyte. Combined with rate performance curve, the spherical carbon with high specific surface area and good multi-level pore structure, showed excellent high current performance and cycle performance.

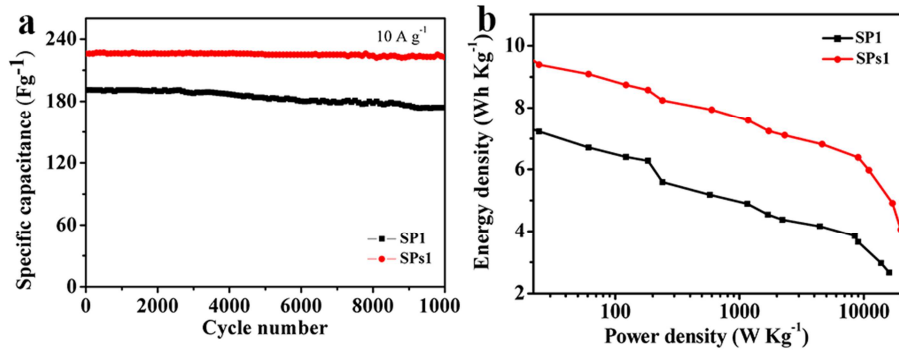


Figure 5. (a) Cycle performance of SPs1 and SP1 electrodes in 6 M KOH at the current density of 10 A g^{-1} ; (b) a Ragone plots of symmetric capacitors in a 6 M KOH solution.

3.2.2. Electrochemical Performance in Organic Electrolyte

For exploring the overall performance of the SPs electrodes, the electrochemical performances of the SPs1 and SP1 electrodes were then studied in 1 M TEABF₄/PC solution, as shown in Figure 6. For the organic electrolyte, the SPs1 electrodes performed better than SP1, the CV curve of SPs1 has nearly perfect rectangular voltammogram shapes even at high scan rate of 200 mV s^{-1} in organic electrolyte (Figure 6a), demonstrating the excellent ion transport behavior even in a viscous electrolyte. Combined with the GCD profiles (Figure 6b), the SPs1 electrodes showed a triangular shape with a small voltage drop (IR) at high current densities, further confirming double-layer capacitance [23]. The IR in SP1 electrodes is more obvious than SPs1, owing to the relatively large volumes in the small micropore [24]. As the specific capacitance is mostly contributed by the meso- and

macropores at high scan rates [25], the SPs1 electrodes with more mesopores showed fast charge and ion propagation, and the GC curves consume a longer time (Figure 6b), which implies a higher specific capacitance. The SPs1 electrodes with reasonable pore size distribution possess a higher specific capacitance of 154 F g^{-1} at 0.05 A g^{-1} (Figure 6c), better than that of SP1 (128 F g^{-1} at 0.05 A g^{-1}), suggesting that the relatively larger mesopores can facilitate faster ion transport to enhance the electrochemical performance [26]. In addition, due to the virtue of good capacitive endurance for double layer capacitance at a large current load, the specific capacitance retentions of the SPs1 and SP1 are 61% and 47% even at a high current density of 10 A g^{-1} , respectively. Furthermore, the capacity deterioration of SPs1 was less than 5.0% after 10,000 cycles (Figure 6d), indicating excellent long-term cyclic stability as a working electrode.

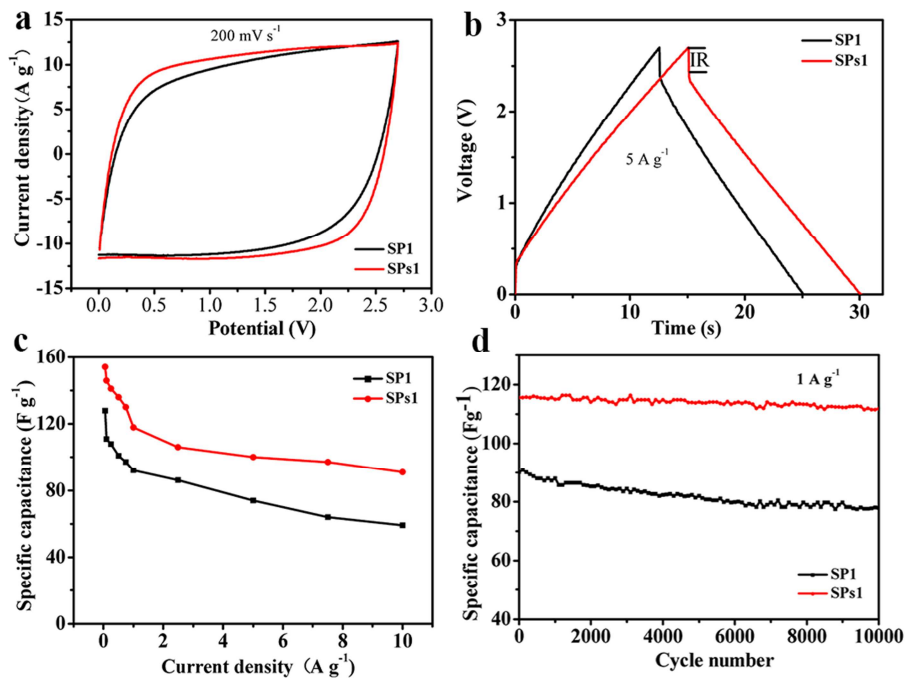


Figure 6. Electrochemical properties of the SPs samples as electrodes in a 1 M TEABF₄/PC solution: (a) CV curves at the scan rate of 200 mV s^{-1} , (b) GCD curves at current density of 5 A g^{-1} , (c) capacitances as a function of current densities and (d) cycle lives at a current density of 1 A g^{-1} .

4. Conclusions

In summary, activated carbon with good sphericity was prepared by simple solvent evaporation method, followed by carbonization and KOH activation under mild conditions. This synthesis process is convenient and environment friendly for high-yield preparation of SPs materials. In addition, compared with the powder activated carbon, the spherical activated carbon has more reasonable pore distribution, which is beneficial to the rapid ion transmission. Remarkably, the SPs1 electrodes behaved superiorly high-performance in both aqueous and organic electrolytes. It shows that the relatively more mesopores can greatly improve the rate performance when the specific surface area is constant. Our results open new possibilities for exploitation of suitable biomass derived carbons as promising electrode materials.

Acknowledgements

This study was supported by the National Natural Science Foundation of China (NSFC 51172160).

References

- [1] Y. Guo, L. Yu, C. Y. Wang, Z. Lin, X. W. Lou, Hierarchical Tubular Structures Composed of Mn-Based Mixed Metal Oxide Nanoflakes with Enhanced Electrochemical Properties. *Advanced Functional Materials* 2015, 25 (32): 5184-5189.
- [2] Z. B. Lei, J. T. Zhang, X. S. Zhao, Ultrathin MnO₂ nanofibers grown on graphitic carbon spheres as high-performance asymmetric supercapacitor electrodes. *Journal of Materials Chemistry*, 2012, 22 (1): 153-160.
- [3] Z. H. Hou, X. H. Li, E. H. Liu, Z. Q. He, et al. New mesoporous carbons prepared by a simultaneous synthetic template carbonization method for electric double layer capacitors. *New carbon materials*, 2004, 19 (1): 11-15.
- [4] C. Merlet, B. Rotenberg, P. A. Madden, et al. On the molecular origin of supercapacitance in nanoporous carbon electrodes. *Nature Materials*, 2012, 11 (4): 306-310.
- [5] P. Staiti, A. Arenillas, F. Lufrano, et al. High energy ultracapacitor based on carbon xerogel electrodes and sodium sulfate electrolyte. *Journal of Power Sources*, 2012, 214 (4): 137-141.
- [6] M. Chen, C. Yu, S. H. Liu, X. Fan, X. Zhao, J. S. Qiu, Micro-sized porous carbon spheres with ultra-high rate capability for lithium storage. *Nanoscale*, 2015 7: 1791-1795.
- [7] X. J. He, H. B. Zhang, H. Zhang, X. J. Li, N. Xiao, J. S. Qiu, Direct synthesis of 3D hollow porous graphene balls from coal tar pitch for high performance supercapacitors. *Journal of Materials Chemistry A*, 2014, 2: 19633-19640.
- [8] M. Seredych, D. Hulicova-Jurcakova, G. Q. Lu, T. J. Bandoz, Surface functional groups of carbons and the effects of their chemical character, density and accessibility to ions on electrochemical performance. *Carbon*, 2008, 46: 1475-1488.
- [9] F. B. Li, Q. L. Qian, F. Yan, G. Q. Yuan, Nitrogen-doped porous carbon microspherules as supports for preparing monodisperse nickel nanoparticles. *Carbon*, 2006, 44: 128-132.
- [10] Y. G. Zhang, C. Y. Wang, P. Yan, Progress in Preparation and Application of Pitch-based Spherical Activated carbon. *Materials Review*, 2002, 2 (16): 46-48.
- [11] J. Tang, J. Liu, C. L. Li, et al. Synthesis of Nitrogen-Doped Mesoporous Carbon Spheres with Extra - Large Pores through Assembly of Diblock Copolymer Micelles. *Angewandte Chemie International Edition*, 2015, 54 (2): 588-593.
- [12] Y. K. Lv, L. H. Gan, M. X. Liu, W. Z. Xiong, J. Xu, D. Z. Zhu, et al. A self-template synthesis of hierarchical porous carbon foams based on banana peel for supercapacitor electrodes. *Journal of Power Sources*, 2012, 209: 152-157.
- [13] Z. J. Qiao, M. M. Chen, C. Y. Wang, Humic acids-based hierarchical porous carbons as high-rate performance electrodes for symmetric supercapacitors. *Bioresource Technology*, 2014, 163: 386-389.
- [14] Y. Z. Ma, B. J. Yu, Y. Guo, et al. Facile synthesis of biomass-derived hierarchical porous carbon microbeads for supercapacitors. *Journal of Solid State Electrochemistry*, 2016, 1-10.
- [15] L. F. Chen, X. D. Zhang, H. W. Liang, M. G. Kong, Q. F. Guan, P. Chen, Z. Y. Wu, S. H. Yu, Synthesis of nitrogen-doped porous carbon nanofibers as an efficient electrode material for supercapacitors, *ACS Nano*, 2012, 6: 7092-7102.
- [16] I. Michio, K. Hidetaka, T. Osamu, Carbon materials for electrochemical capacitors. *Journal of Power Sources*, 2010, 195 (24): 7880-7903.
- [17] P. Chen, D. D. Chung, Dynamic mechanical behavior of flexible graphite made from exfoliated graphite. *Carbon*, 2012, 50 (1): 283-289.
- [18] S. G. Hashmi, J. Halme, T. Saukkonen, E. Rautama, P. Lund, High performance low temperature carbon composite catalysts for flexible dye sensitized solar cells. *Physical Chemistry Chemical Physics*, 2013, 15 (40): 17689-17695.
- [19] V. Ruiz, A. G. Pandolfo. High-frequency carbon supercapacitors from polyfurfuryl alcohol. *Journal of Power Sources*, 2011, 196 (18): 7816-7822.
- [20] K. Kierzek, E. Frackowiak, G. Lota, G. Gryglewicz, J. Machnikowski. Electrochemical capacitors based on highly porous carbons prepared by KOH activation. *Electrochim Acta*, 2004, 49 (4): 515-23.
- [21] Y. Z. Ma, Y. G. et al. Biomass-derived dendritic-like porous carbon aerogels for supercapacitors. *Electrochim Acta*, 2016, 210: 897-904.
- [22] Z. B. Lei, N. Christov, L. L. Zhang, X. S. Zhao. Mesoporous carbon nanospheres with an excellent electro capacitive performance. *Journal of Materials Chemistry* 2011, 21 (7): 2274-2281.
- [23] Y. M. Tan, C. F. Xu, G. X. Chen, Z. H. Liu, M. Ma, Q. J. Xie, N. F. Zheng and S. Z. Yao, Synthesis of Ultrathin Nitrogen-Doped Graphitic Carbon Nanocages as Advanced Electrode Materials for Supercapacitor. *ACS Appl. Mater. Interfaces*, 2013, 5, 2241-2248.

- [24] H. Xu, Q. M. Gao, H. L. Guo, H. L. Wang, Hierarchical porous carbon obtained using the template of NaOH-treated zeolite b and its high performance as supercapacitor, *Microporous Mesoporous Mater* 2010, 133: 106-144.
- [25] Y. T. Li, Y. T. Pi, L. M. Lu, S. H. Xu, T. Z. Ren, Hierarchical porous active carbon from fallen leaves by synergy of K_2CO_3 and their supercapacitor performance, *J. Power Sources* 2015, 299: 519-528.
- [26] Y. Liu, Z. Wang, W. Teng, H. Zhu, J. Wang, A. A. Elzatahry, D. Y. Zhao, A template-catalyzed in situ polymerization and co-assembly strategy for rich nitrogen-doped mesoporous carbon. *Journal of Materials Chemistry*, 2018, 6 (7): 3162-3170.